Limnol. Oceanogr., 52(1), 2007, 204–216

Suspended minerogenic particles in a reservoir: Light-scattering features from individual particle analysis

Feng Peng[1] *and Steven W. Effler*
Upstate Freshwater Institute, P.O. Box 506, Syracuse, New York 13214

Abstract

Light-scattering attributes of minerogenic particles in a reservoir, where these particles dominate over a wide range of light-scattering levels, were characterized by an individual particle analysis technique, scanning electron microscopy interfaced with automated X-ray microanalysis and image analysis (SAX). SAX provided characterizations of the elemental X-ray composition, shape, number concentration (*N*), particle size distribution (PSD), and projected area per unit volume (PAV_m) of these particles. Clay mineral particles represented ~84% of the PAV_m, and they deviated from sphericity more than the other components of the minerogenic assemblage. Scattering coefficients for minerogenic particles at 660 nm ($b_m(660)$) were estimated directly from SAX results based on Mie theory. Both PAV_m and $b_m(660)$ were strong predictors of the observed wide variations in light scattering. Most of the light scattering in the reservoir was attributable to particles in the size range 2–8 μm. Reasonably good closure is reported for estimates of $b_m(660)$, based on comparisons to in situ measurements of the beam attenuation coefficient at 660 nm. The widely used hyperbolic (or Junge) model (to describe PSDs) failed to accurately represent the total value and the particle size dependency of $b_m(660)$ as calculated from SAX observations, whereas the two-component PSD model (using both components or the "*B*"-component only) succeeded for these two features. SAX offers the opportunity to advance partitioning of scattering between minerogenic and organic particle contributions as well as among constituents of the minerogenic component.

Inorganic (or minerogenic) particles make substantial contributions to light scattering in many freshwater systems (Kirk 1985; Effler et al. 2002*b*; Peng and Effler 2005) and Case 2 (coastal) waters (where the optical properties are influenced and often dominated by dissolved and particulate material of terrestrial origin other than algal cells with their retinue; Morel and Prieur 1977; Mobley et al. 2004) and thus are important with respect to apparent optical properties (AOPs) and remote sensing (Woźniak and Stramski 2004). Partitioning of the total particle scattering coefficient ($b(\lambda)$; m^{-1}), an inherent optical property (IOP), is often represented as the summation of organic ($b_o(\lambda)$) and minerogenic ($b_m(\lambda)$) components:

$$b(\lambda) = b_o(\lambda) + b_m(\lambda) \tag{1}$$

Direct measurements or estimates of $b_m(\lambda)$ to support this partitioning have generally been lacking. Instead, values of $b_m(\lambda)$ have usually been approximated from determinations or estimates of $b(\lambda)$ and $b_o(\lambda)$ (i.e., residual calculations; Keen and Stavn 2000).

The magnitude of $b(\lambda)$ is regulated by four different features of the particle population: particle number concentration (*N*), particle size distribution (PSD) (Jonasz and Fournier 1996; Boss et al. 2001; Risović 2002), particle composition (Babin et al. 2003), and particle shape (Jonasz 1987; Mishchenko and Travis 1994). Values of $b(\lambda)$ have been estimated from *N* and PSD information, or specifications, according to (Babin et al. 2003):

$$b(\lambda) = \frac{\pi}{4}\int_{d_{\min}}^{d_{\max}} F(d)Q_b(\lambda,d)d^2\Delta d \tag{2}$$

where $F(d)$ is the PSD function, $F(d)\Delta d$ is the number of particles in the size interval of Δd ($d \pm 1/2\Delta d$) per unit volume, d is particle size, $Q_b(\lambda, d)$ is the (dimensionless) scattering efficiency factor (as a function of λ and d, determined from Mie or other light-scattering theories), and $d_{\min}$ and $d_{\max}$ are the size limits of the calculations. Such calculations are highly sensitive to the shape of the PSD (Babin et al. 2003) and the functional representation adopted for $F(d)$. Inherent assumptions in such calculations usually include (1) the irregularly shaped and randomly oriented particles of natural assemblages scatter light like spherical particles (notably when using Mie theory to calculate Q_b) and (2) particles are compositionally homogeneous (i.e., uniform refractive index).

Characterization of particle composition has been lacking in the context of light scattering (Babin et al. 2003). Measurements are limited mostly to bulk or aggregate properties of the particle populations, such as total suspended solids (e.g., Babin et al. 2003) and volatile and non-volatile (i.e., residual after 550°C) fractions (Vant

[1] Corresponding author (fpeng@upstatefreshwater.org).

Acknowledgments

This study was funded by the New York City Department of Environmental Protection. Field measurements and sampling were performed by B. A. Wagner, M. E. Spada, and A. R. Prestigiacomo. Comments made by Alan Weidemann and anonymous reviewers are greatly appreciated. The C code for Mie scattering calculation, originally translated from FORTRAN (Bohren and Huffman 1983) by Piotr J. Flatau of University of California, San Diego, was adapted to the C++ code compiled for this work. Prof. James Fawcett of Syracuse University is acknowledged for making public his file navigation routine (in C++) that aided the data processing. This is contribution 244 of the Upstate Freshwater Institute.

and Davies-Colley 1984; Gallegos et al. 1990). In contrast, characterization of PSDs has received extensive attention in marine environments (Jonasz and Fournier 1996). Several functional representations of PSDs have been used for marine particles, including the hyperbolic model (power law or Junge distribution), the lognormal distribution (Lambert et al. 1981), the two-component model (Risović 1993), and segmented lognormal (Jonasz and Fournier 1996) or hyperbolic (Risović and Martinis 1995) distributions. The hyperbolic distribution was supported in earlier studies that employed electronic particle counters (e.g., Bader 1970; Carder et al. 1971) and is widely invoked in modeling the underwater light field of marine systems (e.g., Boss et al. 2001; Twardowski et al. 2001; Babin et al. 2003) as well as in inversion algorithms to estimate bulk refractive index and discriminate particle types (Twardowski et al. 2001; Sullivan et al. 2005).

A more rigorous and robust approach for natural heterogeneous particle populations of varying PSD characteristics would consider the light-scattering attributes of individual particles to estimate $b(\lambda)$ or its components:

$$b(\lambda) = \sum_{i=1}^{N} Q_{b,i}(m_i,\lambda,d_i)\mathrm{PA}_i \quad (3)$$

where $Q_{b,i}$ is the scattering efficiency of particle i with projected area PA_i. The value of $Q_{b,i}$ depends on the particle's relative (to water) refractive index ($m = n - in'$, where n and n' are the real and imaginary parts of the complex index of refraction, respectively), its size (d_i), and wavelength (λ). Progress on this forward problem (Sullivan et al. 2005) has been impeded by the lack of adequate individual particle information. Commonly used particle counters (Jonasz 1987; Agrawal and Pottsmith 2000) cannot support such an individual particle approach because no composition (therefore m) information is available. Additional limitations of such instrumentation include the inability to detect submicron particles and the assumption of sphericity for all particles. Scanning electron microscopy (SEM) provides detailed morphometrical information and extends the lower size threshold into submicron sizes (Jonasz 1987; Mobley 1994). Integration of an electron microprobe technique with SEM supports elemental and morphometric characterization of inorganic marine particles (Lambert et al. 1981). However, the populations (both the number of samples and the number of particles in each sample) characterized through such manual SEM techniques have been too small to advance the forward problem.

SEM interfaced with automated X-ray microanalysis and image analysis (SAX) can assess PA_i, d_i, elemental X-ray composition (thus the geochemical type and m_i), and shape for large numbers of inorganic particles over relatively short intervals (Johnson et al. 1991; Peng et al. 2002). This capability can support direct calculations of $b_m(\lambda)$ (Eq. 3) and thereby the partitioning of $b(\lambda)$ according to organic and inorganic components (Eq. 1). Heretofore, applications of SAX have focused on either assessing origins of particles based on composition (Yin and Johnson 1984; Johnson et al. 1991; Effler et al. 1992) or establishing empirical relationships between the total projected area of inorganic particles per unit volume of water ($\mathrm{PAV_m}$; the summation of PA_i for N mineral particles) and AOPs (Effler et al. 2002*a*,*b*; Peng and Effler 2005).

This study documents the application of SAX to characterize the dynamics of light-scattering attributes of minerogenic particles in a reservoir where these particles dominate $b(\lambda)$. Specifically, features of PSD, elemental composition, shape, and $\mathrm{PAV_m}$ are reported. Our objectives are to (1) demonstrate $\mathrm{PAV_m}$ as a strong predictor of surrogate metrics of scattering in this system, (2) test the adequacy of SAX observations for computing $b_m(\lambda)$ from single particle optics and thereby advance the implementation of the forward method (Eq. 3) and the partitioning of $b(\lambda)$ according to minerogenic and organic components (Eq. 1), and (3) characterize PSDs in this system, resolve contributions to $b_m(\lambda)$ according to sizes of minerogenic particles, and evaluate the performance of selected PSD functions within the context of implications for estimates of $b_m(\lambda)$.

Methods

Test system—Schoharie Reservoir (42°22′N, 74°26′W) is one of 19 reservoirs that supply water to New York City. The reservoir, originally filled in 1927, is 8 km long and lacks dendritic complexities (Fig. 1). It has a surface area of 4.6 km^2, a volume of 79×10^6 m^3, and a maximum depth of 41 m when full. The reservoir often experiences drawdown of its surface, measured as changes in water surface elevation (WSE; m) in response to withdrawals for the water supply in excess of runoff inputs from its 815-km^2 watershed.

This is a good test system to evaluate the performance of SAX in specifying the light-scattering effects of inorganic particles because of their dominance of the overall particle assemblage (Effler et al. 2002*b*). Increases in levels of the beam attenuation coefficient at 660 nm ($c(660)$) in the reservoir from runoff events and sediment resuspension are attributable to terrigenous inputs (Effler et al. 2006). The major external source of terrigenous inputs, Schoharie Creek, enters at the southern end of the reservoir (Fig. 1). Maximal levels of $c(660)$ are observed in subsurface layers following summertime and fall runoff events because the terrigenous particles enter in plunging density currents (Effler et al. 2006). Chlorophyll *a* concentrations are relatively low; the long-term average is <3 μg L^{-1} (Effler et al. 2002*b*). The volatile fraction of suspended solid (VSS) is usually less than 10% of the total (TSS); the average VSS/TSS reported for depositing sediment is 0.05 (Effler et al. 2001*b*).

Sampling, drivers, and surrogate measures of light scattering—Samples were collected weekly from two reservoir sites (site 3, an up-reservoir location, and site 1, a down-reservoir location; Fig. 1), at 5-m-depth intervals, over the study period of 16 September through 28 October 2002. A total of 53 samples were collected for laboratory particle and turbidity (T_n, Hach®, model 2100AN; Clesceri et al. 1998) analyses. Drivers of both drawdown and runoff were

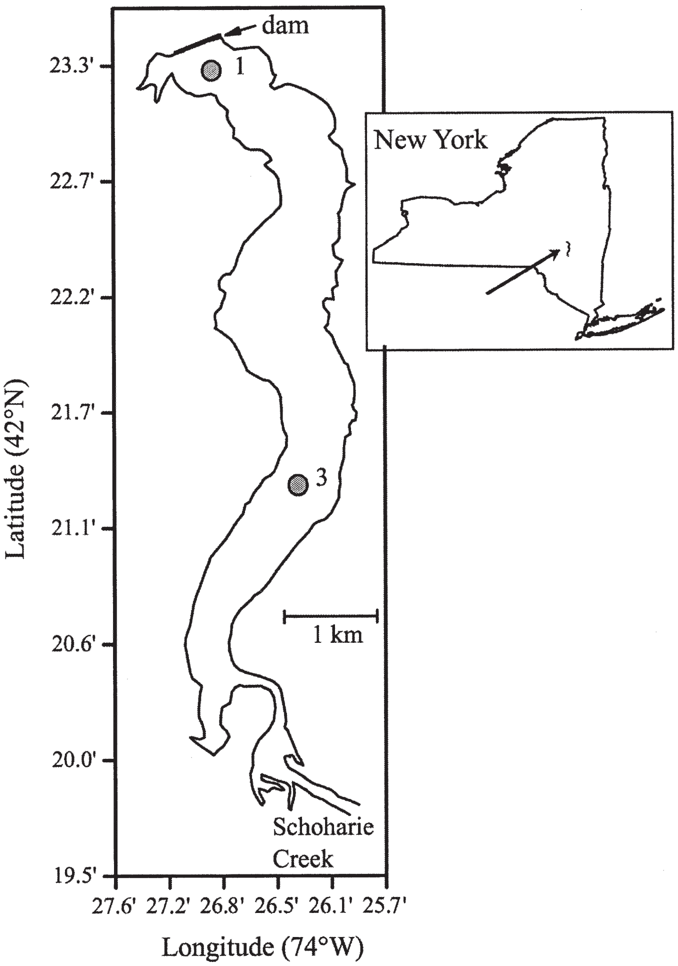

Fig. 1. Map of Schoharie Reservoir (New York, USA), with two sampling sites (up-reservoir site 3 and down-reservoir site 1) and mouth of Schoharie Creek.

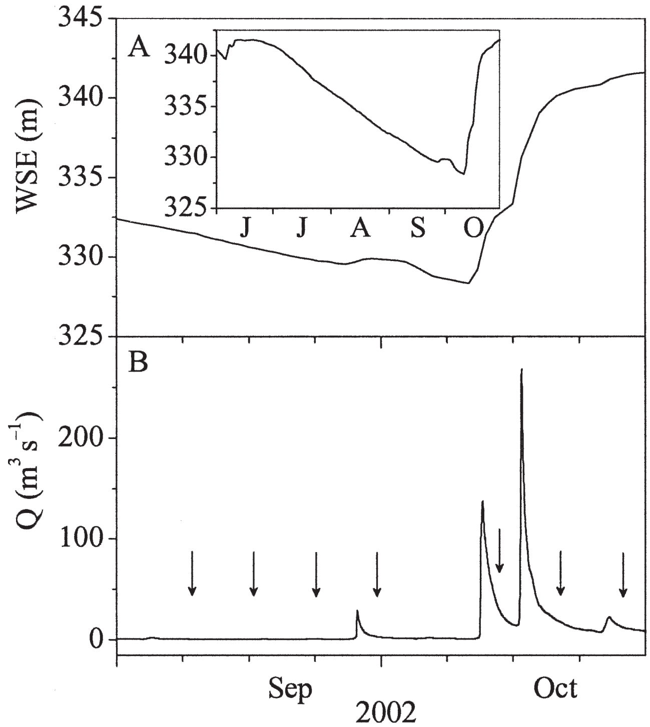

Fig. 2. Time series of hydrologic conditions during study interval of September–October 2002: (A) WSE, with inset extending the time interval to June–October, and (B) flow rate (Q) at mouth of Schoharie Creek, with arrows indicating sampling days.

operative over the study interval (Fig. 2). Drawdown, which had commenced in June (Fig. 2A), was extensive over the September through early October interval. The minimum WSE was the eighth lowest over the 1980–2004 period. Major runoff events occurred on 12 and 16 October (Fig. 2B); these ranked tenth and eleventh highest for October over the 1980–2004 period. The WSE increased 12 m in 10 d in response to these events (Fig. 2A). Three surrogate metrics of $b(\lambda)$ were measured in this study, namely, T_n (NTU), $c(660)$ (m^{-1}), and "optical" backscattering (OBS; BU). T_n, as assessed with a nephelometer, measures light scattered from a beam within a wide angle centered on 90° (Kirk 1994; Davies-Colley and Smith 2001). Beam attenuation coefficient at 660 nm ($c(660)$; C-Star/Wet Labs; path length of 10 cm, effective range 0–15 m^{-1}, resolution of 0.03 m^{-1}) quantifies the fraction of collimated light received in the forward direction (Kirk 1994). OBS (OBS-3; D&A Instruments; effective range 0–250 BU, accuracy of 0.5 BU, resolution of 0.06 BU) measures backscattered light over the 140–160° range. Measurements of $c(660)$ and OBS were made in situ with profiling instrumentation (SeaBird® SeaLogger Profiler). Eight measurements per second were collected during profiling. The instrumentation was lowered at a rate of ~0.5 m s^{-1}; that is, approximately 16 measurements were made over each meter of depth.

SAX protocols—Sample preparation and analytical procedures for SAX characterizations have been described previously (Peng et al. 2002; Peng and Effler 2005). Suspended particles were deposited onto polycarbonate membranes (25-mm diameter, 0.4-μm pore size) by pressure filtration and then carbon coated (thickness ~40 nm) before analysis. To ensure proper loading (monolayer) of particles on the filter membranes, volumes of filtered water were adjusted (generally no more than 25 mL) according to T_n measurements. SAX was conducted with an Aspex® Microanalysis System with Perception™ Analysis Software (with a plug-in Automated Feature Analysis module; AFA). About 1,000 particles (>0.2-μm diameter, based on the electron beam search step size) were analyzed for combined elemental and morphometric characterizations for each of the 53 samples (~2 h instrument time per sample).

The SAX procedure provides chemical characterization of individual particles based on acquisition of X-ray counts for 16 elements (Na and higher atomic numbers, including Al, Si, Fe, and Mn). Elemental composition of a particle is represented by its normalized elemental X-ray counts, that is, relative intensities. Particles were biogeochemically classified into seven generic types (Table 1) according to a scheme developed earlier for this reservoir and other local systems (Peng et al. 2002): "Organics," "Clay," "Si-rich," "Quartz," "Fe/Mn," "Diatom," and "Other" (miscellaneous particles whose elemental X-ray composition does not fit into the criteria of one the specified types). The scheme is consistent with the mineralogy, geochemistry, and origins of particles for the study systems (Peng et al. 2002, 2004). Elemental X-ray relative intensities are the primary criteria used for the classification; for example, the "Clay" (clay minerals, aluminosilicates) class requires that relative intensities of Al and Si be in the ranges 5–55% and 20–85%, respectively (Table 1). More complex classification schemes (i.e., more particle classes) have been used for SAX results from other system(s) (e.g., Yin and Johnson 1984), but these are accompanied by greater uncertainty in their specifications of X-ray elemental stoichiometries. The contributions of "Quartz" versus "Diatom" were resolved according to the protocol of Peng et al. (2002), which is based on the lower X-ray count rates and larger size of diatoms compared to those of quartz. The "Organics" class systematically underrepresents the contributions of organic particles because of their composition of low atomic number elements (lower than Na), due to the methodical limitations inherent to SAX (Peng et al. 2002).

Morphometric characterization of particles by AFA is based on a "rotating chord" algorithm. This algorithm finds the centroid of a particle and draws 32 radiating chords from the centroid (i.e., 16 chords through the centroid) at approximately 11° intervals. Lengths of the 16 chords are measured. The "nonsphericity" of a particle (e.g., shape factor) is represented by the aspect ratio (ASP; Russ 1998):

$$\mathrm{ASP} = \frac{D_{\max}}{D_{\mathrm{perp}}} \tag{4}$$

where $D_{\max}$ is the length of the longest chord through the centroid to the edges of a feature and D_{perp} (or width) is the length of the chord perpendicular to the longest chord. With the chords defined and measured, a particle is represented by a series of triangles rotating around the centroid; PA is the total of all the triangular areas. PAV was the sum of individual PA_i values divided by the volume of filtered water sample. Another commonly used shape parameter to describe the deviation of a particle shape from spherical, form factor (FF; Russ 1998), is also presented. It is calculated as

$$\mathrm{FF} = \frac{4\pi \cdot \mathrm{PA}}{\mathrm{perimeter}^2} \tag{5}$$

For each sample, the mean values of these two morphometry statistics were calculated for three particle groupings: "Clay," non-"Clay" (all minerogenic particles except "Clay" particles), and "Quartz" (a component of the non-"Clay"). Particle size (d), defined as area equivalent diameter, is calculated from PA assuming circular geometry.

PSDs—The PSD function, $F(d)$, is defined by

$$F(d) = \frac{dN}{\Delta d} \tag{6}$$

where dN is the number of particles per unit volume in the size range (Δd) of $d \pm 1/2\Delta d$. Logarithmically spaced size intervals (or "bins") were defined. Twenty-one bins were established from 1.25 to 40.5 μm, coinciding with those used for the LISST particle sizer and counter (Agrawal and Pottsmith 2000). Another 12 bins were established to cover the range 0.2–1.25 μm, adopting the same ratio of the upper to lower bin limits (1.1801) that defines the bin limits for the larger sizes.

Three functions (models) were applied to describe PSDs in the study system. According to the two-component (2C) model (Risović 1993), PSDs are represented by the summation of small (e.g., <1 μm) and large particle components, "A" and "B":

$$F(d) = C_A d^{-\mu_A} \exp(-b_A d^{\gamma_A}) + C_B d^{-\mu_B} \exp(-b_B d^{\gamma_B}) \tag{7}$$

where C_i ($i = A, B$) are constants directly related to the particle concentration N and μ_i, b_i and γ_i are parameters of the distribution. Values of $b_A = 52$ and $b_B = 17$, reported as optimal by Risović (1993), were adopted here. The other six coefficients were allowed to vary in PSD fittings. The second function applied was the "B"-component of the 2C model (2C-B; second part of Eq. 7), also described as the generalized gamma distribution (Risović 1993). Fittings of the 2C-B model (with all four coefficients varying) were applied to d observations $\geq$0.9 μm. Finally, the PSD data

Table 1. Specification of generic particle types, according to X-ray characteristics. All percentages are elemental X-ray relative intensities. Live X-ray acquisition time was 3 s. The "Organics" component is a systematic underestimation of organic particles due to instrument limitation (Peng et al. 2002). The X-ray density in the "Quartz" and "Diatom" specifications refers to the ratio of a particle's total X-ray counts to its size (Peng et al. 2002). The "Other" class incorporates all inorganic particles not captured in the specified classes.

Type	Description	X-ray characteristics	Sources/origins
Organics	Biological	Low X-ray net counts ($\leq$750)	Autochthonous/ terrigenous
Clay	Aluminosilicates	Al, 5–55%; Si, 20–85%; Al plus Si $\geq$ 50%	Terrigenous
Si-rich	Si-containing minerals, silicates	60% $\leq$ Si < 90%	Terrigenous
Quartz	Mineral SiO_2	Si $\geq$ 90%, high X-ray density	Terrigenous
Fe/Mn	Fe/Mn-rich	Fe plus Mn $\geq$ 50%	Autochthonous/ terrigenous
Diatom	Biogenic SiO_2	Si $\geq$ 90%, low X-ray density	Autochthonous
Other	Miscellaneous particles	not specified	Various

were fitted with the widely adopted Junge model (J), described by

$$F(d) = Cd^{-j} \tag{8}$$

where C is a constant depending on N and j is the slope of the distribution. Fitting of the Junge model was performed only for particles with $d \geq 1.25$ μm, the lower threshold for the LISST, and within the common range of lower thresholds for Coulter counters. In these models, d is expressed in dimensionless units, whereas the concentration (N) constant has units of L^{-1} $\mu\mathrm{m}^{-1}$.

Scattering coefficient and its size distribution—Values of $b_m(\lambda)$ were computed using Eq. 3 from the SAX results ("Organics" and "Diatom" types excluded). The scattering efficiencies of individual particles ($Q_{b,i}$) were calculated on the basis of Mie theory assuming that all particles were homogeneous spheres. Representative values of n (real part of the complex refractive index relative to water) for most mineral particles are in the range 1.15–1.20 (Woźniak and Stramski 2004), whereas knowledge on the value of n' is limited and uncertain by comparison. Bukata et al. (1995) suggested that the value of n' for mineral particles is on the order of 0.001, while Egan and Hilgeman (1979) reported ~0.0001 (at 666 nm) for pure kaolinite. An n value of 1.17 was used in the Mie calculations for the mineral particles of this reservoir. Three values of n' were used (0, 0.0001, and 0.001) to represent the uncertainties in calculated $b_m(\lambda)$ associated with the uncertainties in n'. Wavelength was specified as 660 nm to support comparisons of $b_m(\lambda)$ at that wavelength to $c(660)$ measurements. The mean scattering efficiency of the minerogenic particles at 660 nm of each sample ($<Q_{b,m}(660)>$) was calculated as the ratio of $b_m(\lambda)$ to PAV_m.

Cumulative $b_m(660)$ as a function of particle size (e.g., Pak et al. 1971; Babin et al. 2003) was determined to resolve the relative contributions of different sizes of minerogenic particles. These results are presented for SAX observations as well as for 2C, 2C-*B*, and J function fits; the calculations for the function fits employed Eq. 2 and serve to illustrate the implications of shortcomings of the functions in representing size class contributions to $b_m(660)$.

Results

Variations in light scattering—Substantial variations in light scattering were captured in the monitoring program; for example, OBS values ranged from ~4 to 54 BU for the SAX sampling depths. The distribution of the OBS observations deviated substantially from normality (Shapiro–Wilk test, $W = 0.67$, $p < 0.0001$); 25% of the observations were >13 BU, and mean and median values were 12.5 and 9.6 BU, respectively.

Both temporal and spatial components contributed to the overall variations in light scattering. This is illustrated in profiles of T_n (Fig. 3A) and OBS (Fig. 3B) on dates preceding (30 September) and following (14 October) the runoff event of 12 October at the down-reservoir site. Major increases in light scattering, localized at subsurface depths as a result of the entry of turbid density currents (Effler et al. 2006), were reflected in the profiles of both surrogate metrics (Fig. 3A,B). Though a much more detailed pattern emerged from the OBS profile, the sampling depths for T_n (and SAX) measurements captured the primary vertical features. Patterns of T_n, $c(660)$, and OBS were highly correlated ($r > 0.94$, $p < 0.0001$, for all paired observations).

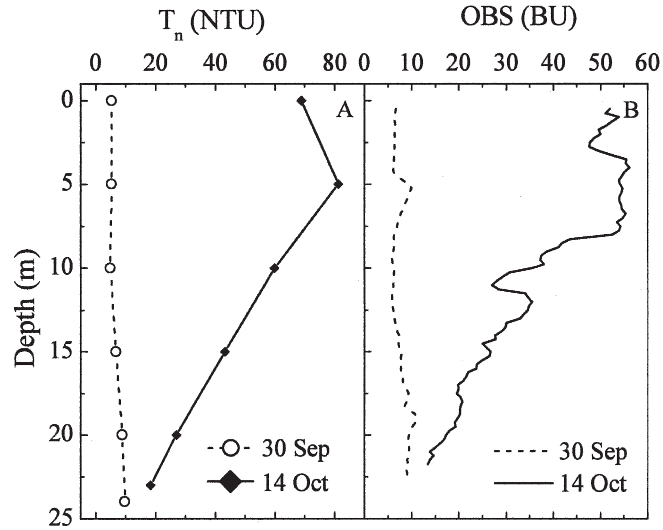

Fig. 3. Features of light scattering conditions at site 1 in Schoharie Reservoir for 2 d bounding a runoff event: vertical profiles of (A) T_n and (B) OBS.

Composition and morphometries of particle populations—The chemical classification scheme, based primarily on elemental X-ray relative intensities (Table 1), performed well in representing the particles of this reservoir, as more than 95% of the particles were in the specified particle types (i.e., not in "Other" category) in the 53 samples. Mineral particles dominated the measured PAV of the reservoir's water column during the study period, representing an average of more than 95% of the total PAV (Table 2). The "Clay" particle class remained uniformly dominant, accounting for nearly 80% of PAV (Table 2) and 84% of PAV_m (i.e., "Organics" and "Diatom" type contributions subtracted from total PAV), on average. "Quartz" was the second-largest contributor to PAV_m, corresponding to about 8%. Despite the wide variations in the magnitude of scattering, the particle type composition of the minerogenic particle population of this reservoir remained relatively uniform. The composition of PAV_m corresponds closely to the average reported for Schoharie Creek based on earlier monitoring (Peng et al. 2004) and establishes the terrigenous origins of the suspended particulate material.

Both representations of particle shape, ASP and FF, indicated that nonspherical morphometries prevailed for the minerogenic particles of this system; average values were significantly different from those for spheres (i.e., ASP > 1, FF < 1, $p < 0.0001$; Table 3). No systematic dependence of these representations of shape on size (d) was observed. The deviations from sphericity were signif-

Table 2. Summary of projected area per unit volume (PAV) magnitude and composition (mean ± standard deviation) of particle populations for Schoharie Reservoir during the study interval.

	Type distribution (%)						
PAV (cm^2 L^{-1})	Organics	Clay	Si-rich	Quartz	Fe/Mn	Diatom	Other
38.2 ± 43.7	3.1 ± 2.2	79.4 ± 3.8	3.6 ± 1.1	7.7 ± 2.7	1.5 ± 0.7	1.2 ± 1.1	3.4 ± 1.7

icantly greater (paired *t*-test, $p < 0.0001$) for the "Clay" component (Fig. 4A–C) compared to the non-"Clay" minerals; the least deviation from sphericity was observed for "Quartz" particles (Table 3; Fig. 4D). Microscopic observations suggested that particle shapes were diverse (e.g., Fig. 4C) in this system.

PSDs of mineral particles—PSDs of mineral particles are presented for four samples (Fig. 5A,B) that bracketed much of the range of encountered conditions. Results for two samples collected from the surface waters at the two sites on 23 September (Fig. 5A) illustrate spatial differences in PSD when the reservoir was extensively drawn down (Fig. 2A). The shallower (water depth of ~3 m) up-reservoir site 3 sample was substantially more turbid (23 NTU) than the sample from the deeper (water depth of ~21 m) down-reservoir site (8.8 NTU) as a result of localized inputs from sediment resuspension, which was promoted by drawdown (Effler and Matthews 2004). Patterns for the other two samples (Fig. 5B), collected on 30 September and 14 October from a 5-m depth at site 1, reflected the effect of the 12 October runoff event on PSD characteristics. The T_n value (81 NTU) was 16-fold greater at this site following the runoff event.

The same general PSD pattern was observed for these four samples (as well as all others collected in this study): frequency peaks at sizes <1 μm (i.e., 0.6–0.8 μm) and more rapid decline in particle numbers for larger than for smaller particles (as compared to the peak frequency sizes). *N* was higher throughout the reported size range for the more turbid samples (Fig. 5A,B). The shapes of the PSDs differed more for the intersite comparison during extensive drawdown (Fig. 5A), with greater relative contributions from particles >4 μm for the sample from the shallower up-reservoir site 3. In contrast, the PSD shapes for the samples collected from the subsurface down-reservoir site 1 before and after the runoff event were similar (Fig. 5B) despite a more than10-fold increase in *N*.

Table 3. Metrics of particle shape (ASP, FF; mean ± standard deviation) for three components of minerogenic particles in Schoharie Reservoir.*

Component	ASP	FF
"Clay"	1.75 ± 0.09	0.60 ± 0.03
"Quartz"	1.38 ± 0.05	0.72 ± 0.02
Non-"Clay" (inorganic)†	1.53 ± 0.11	0.68 ± 0.03

* ASP, aspect ratio; FF, form factor.
† This population includes "Quartz"-type particles.

Fits of the 2C, 2C-*B*, and the J functions to the observed PSDs have been included for the presented distributions (Fig. 5A,B). Constraint of the J fits to sizes greater than a typical lower threshold (1.25 μm) of particle counters was supported by the systematic nonlinearity (on log-log scale) of the PSDs when smaller particles were considered. The values of *j* for these four PSDs ranged from 2.72 to 3.91 (Table 4). The lower *j* value at site 3 reflected relatively greater abundance of larger particles, whereas the higher

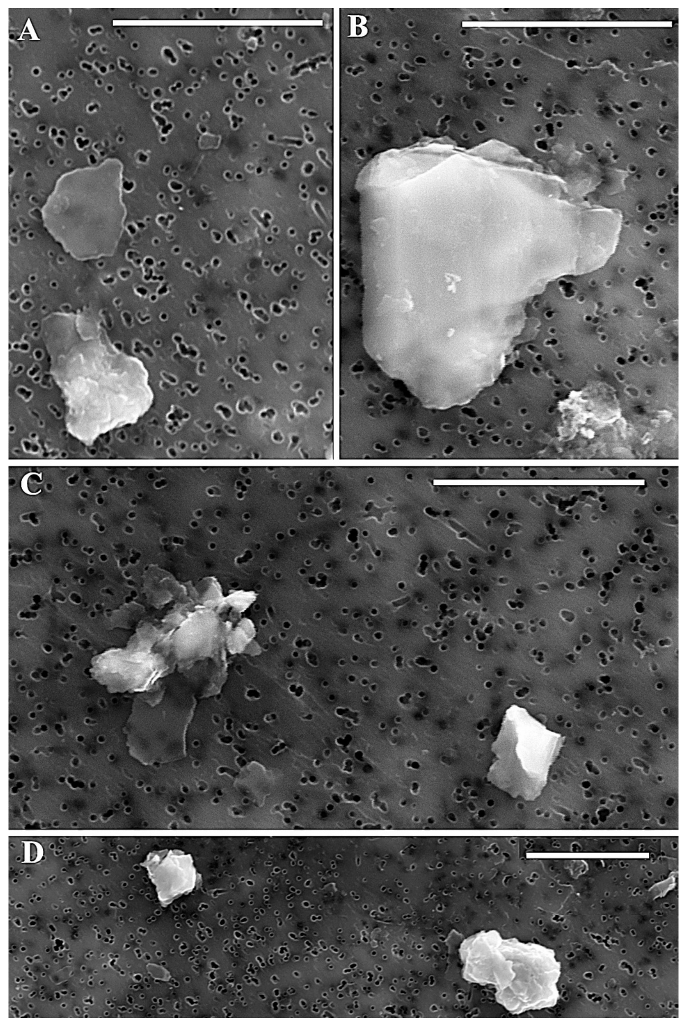

Fig. 4. Micrographs showing particle morphometries observed in Schoharie Reservoir during the 2002 study interval: (A) and (B) plate-like clays, (C) and (D) irregular clays and quartz, respectively. Particles in (A) and (D) were collected at site 1 at 5-m depth on 14 October, and those in (B) and (C) were collected at surface layer of site 3 on 23 September. The bar in each micrograph is equivalent to 10 μm.

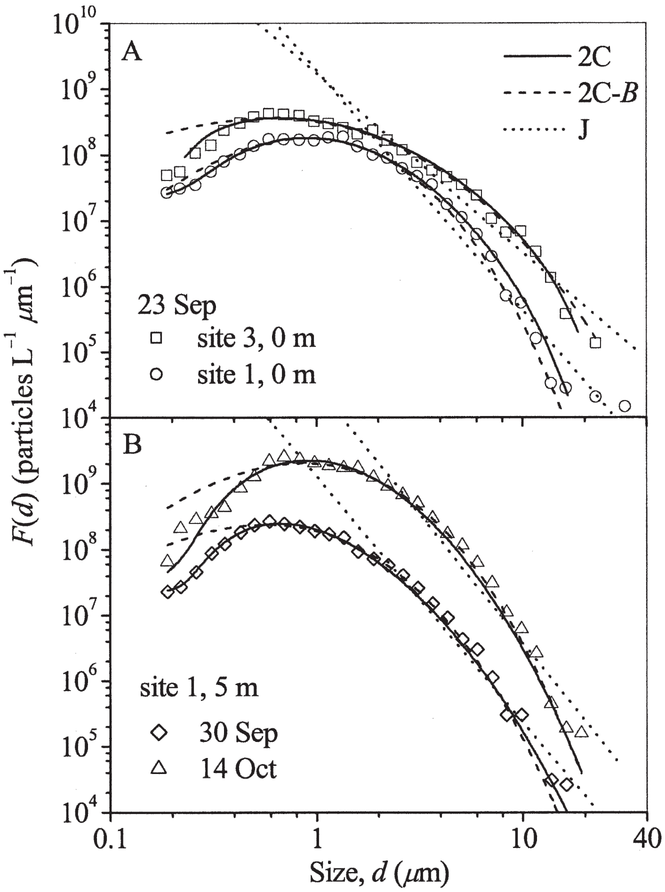

Fig. 5. Selected size distributions of mineral particles in Schoharie Reservoir: (A) 23 September, site 3 and site 1, surface waters, and (B) site 1, 5-m depth, 30 September and 14 October. 2C, 2C-*B*, and J function fittings are shown for each sample; the 2C-*B* was fitted to particle $\geq$0.9 μm, the J model to particles $\geq$1.25 μm.

values obtained for the other three samples were more similar to those commonly reported and invoked for most marine particle populations (j = 4; Babin et al. 2003). The J function was not an appropriate representation of the full size spectra of these observations. Further, it had shortcomings for the constrained size interval ($\geq$1.25 μm) of the observed PSDs. Generally, it overpredicted the concentrations of the largest particles (e.g., $\geq$10 μm) and underpredicted those of intermediate sizes (e.g., 3–8 μm). These fits are included in this analysis, however, to demonstrate the interesting implications associated with its adoption for this system (widely used elsewhere) with respect to the size spectra of $b_m(\lambda)$ (subsequently).

The 2C-*B* model fitted well for $d \geq 0.9$ μm, but the concentrations of smaller particles were overpredicted (Fig. 5). The average values of b_B and γ_B (17.3 and 0.281, respectively; Table 4) for the four selected samples of this study were similar to those for marine PSDs, whereas that of μ_B (4.24; Table 4) was more than twofold greater than the value (2) reported as optimal for marine systems by Risović (1993, 2002). The 2C model provided the best fit for the entire size range of observations (Fig. 5); however, the value of C_A was negative (Table 4) in such a fit.

PAV_m, b_m, and $<Q_{b,m}>$—PAV_m was a strong linear predictor of light scattering in this study; at least 89% of the more than 10-fold variations in the three surrogate metrics of scattering (Fig. 6A–C) were explained by the variability in PAV_m. The best performance (r^2 = 0.98) was for T_n. Similarly, the SAX-based estimates of $b_m(660)$ (with n' = 0.001) explained much of the variations in the surrogate measures of scattering; values of r^2 were 0.93, 0.97, and 0.98 for $c(660)$, OBS, and T_n relationships, respectively. The average value of the ratio of the absorbing (due to n' of m) component to scattering for the mineral particles of this

Table 4. Model (2C, 2C-*B*, and Junge; Eqs. 7 and 8) fitting results for four selected mineral particle size distributions (PSDs) for Schoharie Reservoir; coefficient of determination $r^2 \geq 0.95$ in all cases.

Sample specifics				
Date	23 Sep	23 Sep	30 Sep	14 Oct
Site, depth	Site 3, 0 m	Site 1, 0 m	Site 1, 5 m	Site 1, 5 m
T_n (NTU)	23.0	8.8	5.3	81.3
2C fits (b_A = 52, b_B = 17)				
C_A (L^{-1} μm^{-1})	-3.06×10^{30}	-3.70×10^{30}	-2.25×10^{30}	-3.48×10^{31}
μ_A	2.54	6.51	8.05	9.02
γ_A	0.072	0.148	0.222	0.221
C_B (L^{-1} μm^{-1})	9.97×10^{15}	2.78×10^{16}	6.32×10^{15}	7.63×10^{16}
μ_B	3.14	3.34	2.87	4.09
γ_B	0.220	0.256	0.260	0.292
2C-*B* fits				
C_B (L^{-1} μm^{-1})	9.13×10^{15}	6.99×10^{15}	7.05×10^{15}	6.76×10^{16}
μ_B	3.78	4.12	4.11	4.94
b_B	17.17	17.28	17.42	17.32
γ_B	0.246	0.279	0.290	0.302
Junge fits				
C (L^{-1} μm^{-1})	1.74×10^9	1.95×10^9	1.29×10^9	3.09×10^{10}
j	2.72	3.64	3.74	3.91

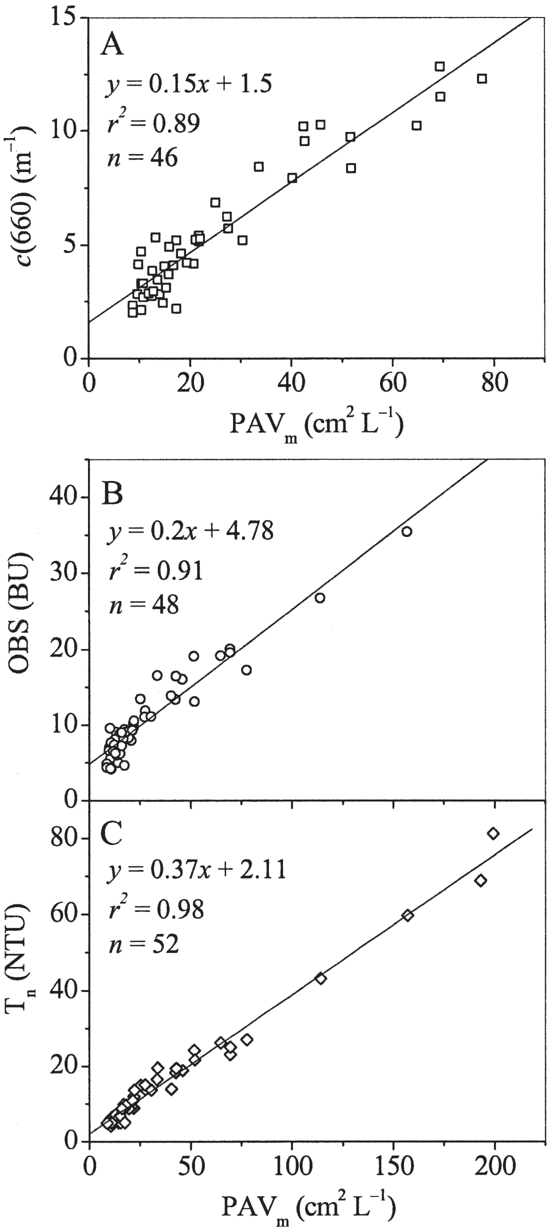

Fig. 6. Evaluation of relationships between surrogate measures of light scattering and PAV_m in Schoharie Reservoir, with linear least squares regression analyses: (A) $c(660)$, (B) OBS, and (C) T_n.

study ranged from 0.004 (for $n' = 0.0001$) to 0.03 (for $n' = 0.001$) at 660 nm.

Calculated $<Q_{b,m}(660)>$ values (with $n' = 0.001$) tended to be somewhat greater than 2.0 for the 53 samples, with mean and median values of 2.30 and 2.33, respectively. The particle assemblages at the up-reservoir site 3 were significantly (two sample t-test, $\alpha = 0.05$, $p < 0.001$) less efficient in scattering light than those at the down-reservoir site 1, with average values of $<Q_{b,m}(660)>$ of 2.25 and 2.32, respectively. These calculations of $<Q_{b,m}(660)>$ were insensitive to more detailed specifications of m according to the various minerogenic particle types because of the similarity of m values for the mineral particles (Woźniak

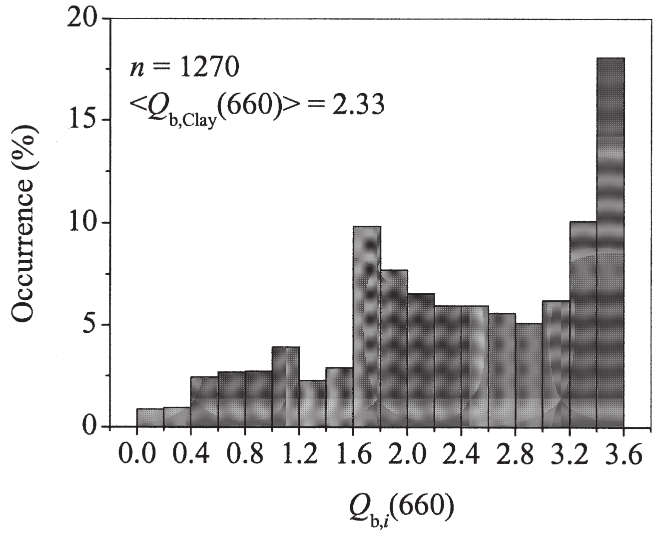

Fig. 7. Distribution of $Q_{b,i}(660)$ values ($m = 1.17 - 0.001i$ in Mie calculations) for clay particles for the sample from site 1, depth of 5 m, on 14 October 2002.

and Stramski 2004) of this reservoir. Further, the mean scattering efficiencies for the different minerogenic particle classes were also similar; the mean values for "Clay" and "Quartz" were 2.28 and 2.42, respectively. These minor differences reflect differences in the PSDs of the classes because of the uniform values of m adopted in the Q_b calculations. Even when a broader range of n (1.1–1.26) was considered, the maximum difference in $<Q_b(660)>$ was less than 5%. The distribution of calculated $Q_{b,i}(660)$ values for the clay particles for the sample from site 1, depth of 5 m, on 14 October (Fig. 7) is generally representative of those obtained for all the study samples: low occurrences for values <1.6, a secondary peak between 1.6 and 1.8, and the primary peak occurrence at the range 3.4–3.6. The corresponding $<Q_{b,Clay}(660)>$ value for this sample, 2.33, reflects the combined effects of $Q_{b,i}$ and PA_i.

Cumulative $b_m(660)$ plots are presented for three samples (Fig. 8), for which PSDs were described previously, to depict the contributions of different size classes. These cases generally bracket those encountered in the study. Contributions by the smallest particles (e.g., <1.5 μm) varied substantially; such particles accounted for <4% of the $b_m(660)$ for the up-reservoir site sample (Fig. 8A) and ~10% in the down-reservoir samples (Fig. 8B,C). Larger particles made greater contributions to $b_m(660)$ at the up-reservoir site; about half of the scattering was caused by particles with $d > 5$ μm. In contrast, particles of similar sizes in the down-reservoir samples contributed only ~20% of the scattering. The size dependency patterns for these two samples were quite similar, despite the 20-fold difference in the total $b_m(660)$. Particles in the d range 1.5–8 μm accounted for ~80% of the $b_m(660)$ in the down-reservoir samples as opposed to 60% at the up-reservoir site.

Discussion

PAV_m and $<Q_{b,m}(660)>$—The wide variations in light-scattering levels encountered in this study and the

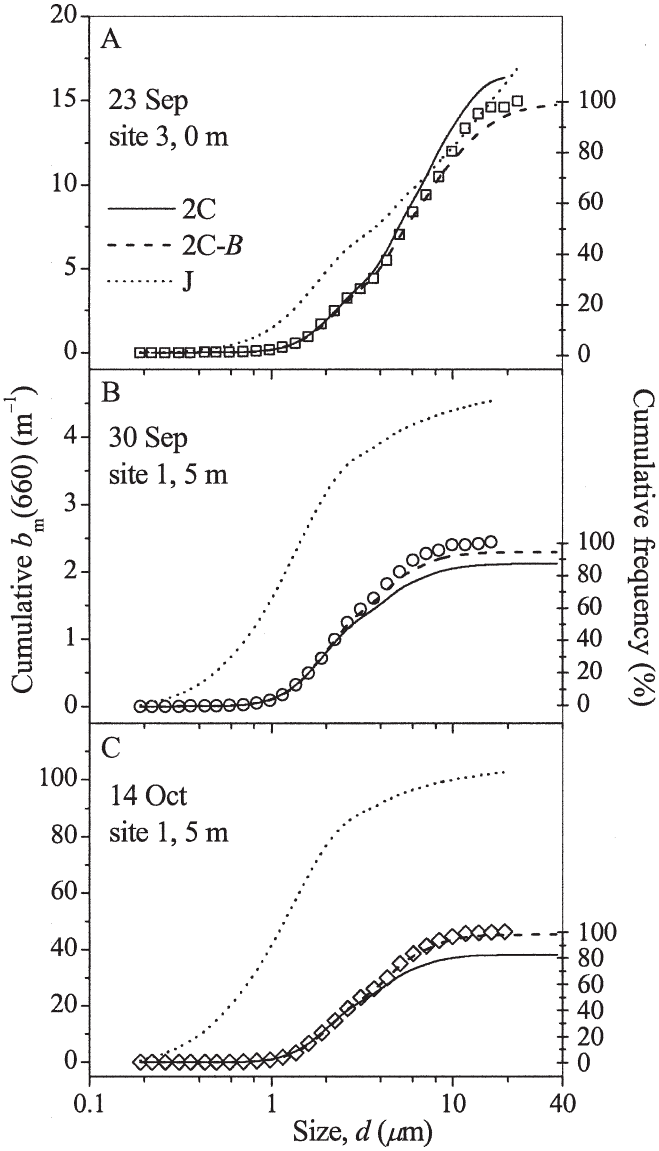

Fig. 8. Cumulative distribution patterns of $b_m(660)$ over particle sizes calculated from SAX results and from 2C, 2C-*B*, and Junge function fittings (with $m = 1.17 - 0.001i$), for three samples: (A) 23 September, site 3, surface; (B) 30 September, site 1, 5 m; and (C) 14 October, site 1, 5 m.

dominance of minerogenic particles offered an opportunity to test the performance of SAX in supporting estimates of $b_m(\lambda)$. PAV_m has been shown to be a strong linear predictor of all three of the used surrogate metrics of light scattering (Fig. 6). This supports the position that variations in the quantity of minerogenic particles largely regulated the observed patterns in light scattering. Further, it substantiates the proposition that the scattering associated with various constituents is proportional to their respective projected particle areas (Eqs. 2 and 3; Owen 1974; Treweek and Morgan 1980). Rarely has this been demonstrated on the basis of the characterization of individual particles (Peng et al. 2004). Several factors probably contributed to the scatter in the relationships between PAV_m and the metrics of light scattering: (1) space–time differences in waters sampled and analyzed in the laboratory (SAX and T_n) versus measured in situ ($c(660)$ and OBS); (2) changes in the relative contributions of organic particles, particularly at lower scattering levels; (3) variations in PSDs and therefore $<Q_{b,m}(660)>$; and (4) uncertainties in both SAX and the surrogate light-scattering measurements. That the relationship between PAV_m and T_n emerged as the strongest ($r^2 = 0.98$; Fig. 6) suggests the first of the previously mentioned factors was probably the most noteworthy, as the T_n and SAX measurements were paired.

The Mie theory stipulation of particle sphericity was not met for the minerogenic particles of this study (Table 3; Fig. 4). This is not unexpected; there appears to be a general recognition that most marine (and presumably freshwater) particles are not spherical (Jonasz 1987; Volten et al. 1998; Gordon and Du 2001). Deviations from sphericity cause substantial shifts in the volume scattering function, particularly in the context of backscattering and side scattering (Mugnai and Wiscombe 1989; Mishchenko and Travis 1994). However, the effect on forward scattering and overall scattering (i.e., intergrated through all angles) is decidedly less (Hollard and Gagne 1970; Mishchenko and Travis 1994; Volten et al. 1998). Other analytical frameworks, such as *T*-matrix (e.g., Mishchenko and Travis 1994), exist to support light-scattering calculations that, to some extent, accommodate the effects of particle shape. These are computationally more demanding and have their own sources of substantial uncertainty (Stramski and Woźniak 2005), particularly with respect to representing real particle shapes as various geometric idealizations (Mishchenko and Travis 1994; Gordon and Du 2001). Mie theory calculations represent a viable albeit imperfect framework to conduct the forward problem in scattering based on individual particle information for thousands of particles that differ in size and shape (e.g., Fig. 4). The extent to which the problem is tractable with more complex frameworks for the particle populations described for this study system is uncertain. The Mie theory framework may have additional advantages for systems that have greater compositional variability than that observed in this study system. Closure analyses of comparing modeled $b(\lambda)$ based on individual particle information to bulk measurements represent a test of the veracity of the particle information as well as the appropriateness of Mie theory calculations.

For spherical mineral particles of the sizes that are important to light scattering, values of $Q_{b,i}(660)$ from Mie calculations lie between 1 and 3.6. Effective values for polydispersed particle populations tend to approach the limiting values of 2 (Bricaud et al. 1983; Jonasz 1987). It is possible that the effective value of $<Q_{b,m}(660)>$ for the particles of this reservoir more closely approaches the limiting value of 2, under the conditions of the water column (e.g., random particle orientation), than indicated by the presented estimates.

Closure for $b_m(660)$ estimates—Comparison of the $b_m(660)$ estimates based on SAX to $c(660)$ values offers a preliminary albeit imperfect basis to evaluate the extent of numeric closure. The populations of $c(660)$ values used in this analysis were generated from the linear least squares

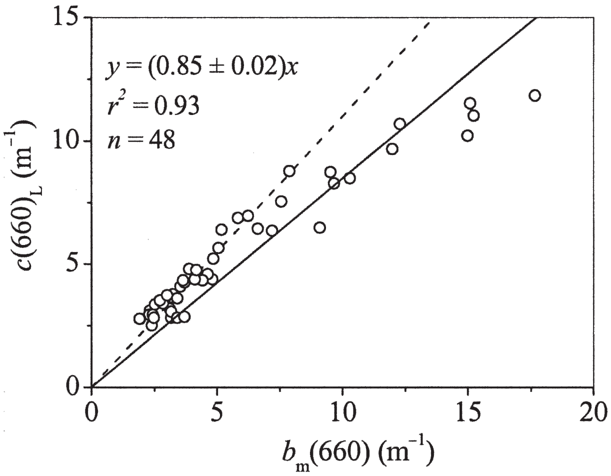

Fig. 9. Evaluation of the relationship between $c(660)_L$ (= $0.41 \times T_n + 0.77$) and $b_m(660)$ (estimated from SAX results with $m = 1.17 - 0.001i$); standard error of the estimated slope is shown. Approximate closure line (dash), corresponding to $c(660) = 1.1 \times b_m(660)$, is added for reference.

regression relationship obtained between field $c(660)$ measurements and the laboratory observations of T_n ($c(660)_L = 0.41 \times T_n + 0.77$, $r^2 = 0.88$). This relationship is very similar to that obtained ($c(660)_L = 0.40 \times T_n + 0.3$, $r^2 = 0.96$) the following year from paired laboratory measurements of ~800 samples from the reservoir, with the same turbidimeter and same model transmissometer (Effler et al. 2006). This manipulation did not substantively alter the subsequently presented analysis but had the effect of reducing the scatter that likely was attributable to the modest disconnect between field and laboratory measurements. Values of $c(660)_L$ should be systematically higher than the actual $b_m(660)$, according to the contribution of $b_o(660)$ (Eq. 1) and the inclusion of $a(660)$ (= $c(660)- b(660)$). The value of $b_o(660)$ is low relative to $b_m(660)$ in this system because of the small contribution of organic particles to the overall particle population and their relatively low m values (Babin et al. 2003). For example, the phytoplankton contribution to $b_o(\lambda)$ would be roughly 0.3 m^{-1} for an average Chl *a* concentration of 3 $\mu g\ L^{-1}$ by the use of a chlorophyll mass specific scattering coefficient of 0.1 $m^2\ g^{-1}$ (e.g., Weidemann and Bannister 1986). Assuming a similar contribution from detritus, $b_o(\lambda)$ would represent ~5–10% of $b(\lambda)$. The value of $a(660)$ is small relative to $c(660)$ in turbid systems such as the study reservoir (e.g., 3–6% in Case 2 marine waters; Babin et al. 2003). Based on these considerations, reasonable closure between independent measures of $c(660)$ and estimates of $b_m(660)$ for this system corresponds to $c(660) = 1.1 \times b_m(660)$.

A strong relationship prevailed between $c(660)_L$ and $b_m(660)$ (Fig. 9). According to linear least squares regression, differences in the SAX-based estimates of $b_m(660)$ explained 93% of the observed variations in $c(660)_L$ ($c(660)_L = 0.85 \times b_m(660)$). The slope is ~23% less than the value targeted for reasonable closure. A modest but distinct curvilinear relationship is apparent between $c(660)_L$ and $b_m(660)$. Many of the lower $b_m(660)$ values (<4 m^{-1}) essentially match the closure target. However, greater relative contributions of $b_o(660)$ to $c(660)$ at these lower $b_m(660)$ levels could be in part responsible for this structure.

At least one factor contributes to the overestimation of $b_m(660)$ and consequently the deviation from closure. PA, and therefore PAV_m, is overestimated by SAX for certain particles as a result of their preferred orientation (lying flat) on the filter (Jonasz 1987). The projected area of a nonspherical particle randomly oriented in a water column (PA*) is smaller than the PA determined by SAX (e.g., Jonasz 1987); thus, PAV_m and $b_m(660)$ (Eq. 3) are overestimated. A PA*/PA ratio value of 0.87 has been reported for quartz dust particles (Proctor and Harris 1974). A lower PA*/PA value for clays of ~0.7 would result in closure here. Such a lower value of the ratio compared to the quartz value is supported by the significantly greater deviations from sphericity observed for the "Clay" particle class compared to "Quartz" (Table 3). The morphometries observed for the "Clay" class particles are qualitatively consistent with the "plate-like" structure (Fig. 4A,B) generally attributed to clay mineral particles, a feature that would result in a lower PA*/PA ratio and that has been identified as responsible for their relative persistence in water columns (Lal and Lerman 1975; Davies-Colley and Smith 2001). An additional factor, not as certain, in overestimation of $b_m(660)$ may be that values of $\langle Q_{b,m}(660)\rangle$ from Mie calculations are too high. If the limiting value of 2 (Bricaud et al. 1983; Jonasz 1987) is adopted for all samples, the best fit (i.e., with $c(660)_L$ regressed against $2 \times PAV_m$) slope value will be 0.96 instead, which falls short of closure by 13% (instead of 23%).

We are encouraged by the extent of closure achieved here in estimating $b_m(\lambda)$ independently based on measurements with SAX in light of the uncertainties in the Mie theory estimates (e.g., deviation from sphericity, modest variability caused by different values of m). The observed performance is generally supportive of this application of Mie theory calculations. However, there appears to be little basis for comparison of the extent of closure reported here. We found no examples in the literature of similar attempts to solve the forward problem for $b(\lambda)$ based on detailed individual particle information for a large population of particles. Iturriaga and Siegel (1989) reported some success in the forward problem for particle absorption.

The extent and character of the differences between SAX-based $b_m(660)$ estimates and $c(660)$ measurements presented here are consistent with the features of the SAX procedure and the reported composition of the particle population. This analysis suggests that greater degree of closure could be achieved on the basis of either more detailed geometric classification of particles (so PA of a particle can be adjusted to PA* based on the degree of its morphometrical deviation from a sphere) or empirical approaches such as paired scattering and SAX measurements for a range of well-defined particle populations. Metrics of particle shape (Table 3) may form a reasonable basis to support particle type-specific estimates of PA*. A similar but opposite adjustment has been attempted to compensate for the underestimated PA from measured volume by a particle counter, associated with the nonsphericity of particles not accommodated by such instruments. Jonasz (1987), based on morphometrical analyses of SEM images of a limited number of particles, applied corrections factors (>1, depending on size) to Coulter counter–derived PAs for a Baltic sample in an effort to reconcile the Coulter particle data with light-scattering measurements; the underestimation by the calculated $b(633)$ according to Eq. 2 was 5% after the correction as compared with 40% when the original counter data were used. Future closure efforts with SAX should be supported by direct bulk measurement of $b(\lambda)$ (Babin et al. 2003). Representative PA* values would lead to orientation-adjusted d values (d*). The corresponding PSDs (e.g., Fig. 5) would be shifted toward smaller particles. A PA*/PA ratio for clays of 0.7 would correspond to a d*/d ratio of 0.84. However, the reported independence of the metrics of particle shape from size indicates that the character (e.g., shape) of the PSDs would remain largely unchanged. As an interim measure, we recommend adoption of a PA*/PA value of 0.7 for clay mineral particles and 0.87 for quartz in the application of SAX to estimate $b_{\mathrm{m}}(660)$.

PSD functions and implications for light scattering—The performance of function fits of PSDs in matching $b_{\mathrm{m}}(\lambda)$ estimates has important implications for inversion efforts seeking to predict PSDs from scattering measurements. The commonly adopted J function had substantial shortcomings in representing the total $b_{\mathrm{m}}(660)$ values and the relative contributions of various sizes (Fig. 8). When constrained to the SAX observed particle size range, the J function matched the calculated total $b_{\mathrm{m}}(660)$ for the 23 September up-reservoir sample reasonably well, but the size trajectory deviated substantially; for example, the contributions of particles in the size range 1–6 μm were overpredicted (Fig. 8A). Such deviations are incongruent with most inversion goals (Twardowski et al. 2001; Stavn and Keen 2004; Sullivan et al. 2005). Further, the J function depicted unrealistic strong increases in $b_{\mathrm{m}}(660)$ beyond the sizes of SAX observations for this sample. Similarly, Stavn and Keen (2004) reported that the J function, while performing poorly in representing the contributions of various sizes, could produce reasonable estimates of total scattering by balancing out the errors for different sizes. The more commonly observed shortcomings of the J function in this study are illustrated for the two down-reservoir samples that bracketed the major runoff event (Fig. 8B,C). The shapes of size trajectories were similar to those based on observations, but the total scattering was overpredicted by a wide margin (about twofold) because of the over-representation of contributions of small particles (Fig. 5). Lambert et al. (1981), in their characterization of marine inorganic particles, also reported that the strongest deviations from the J function were localized below the lower size threshold of Coulter counters. They suggested that the support for the J function was in part an artifact of the limitation of the Coulter counters.

In contrast, both the 2C and the 2C-B functions performed well in representing the size dependency and overall values of $b_{\mathrm{m}}(660)$ (Fig. 8). This similar performance by 2C-B to that of 2C, despite the comparatively inferior fit of 2C-B for submicron particles (Fig. 5), is a manifestation of the minor contribution made by submicron particles to scattering. The 2C-B representation has certain advantages for the PSDs presented here; it avoids the use of a negative value of C_A (Eq. 7; Table 4) that may result in negative $F(d)$ when the function fits are extended beyond the size limits of these observations (e.g., modeling exercises), and it requires fewer number of function coefficients than the 2C does (three if an optimal value of 17 is used for b_B instead of six). Other functions may also be suitable to represent the presented PSDs and associated size trajectories of b_{m}; for example, lognormal function (one or two segments; Jonasz and Fournier 1996) also performed well (not shown) for the samples included in this study.

Implications—The capability of SAX to assess the light-scattering attributes of a large number of inorganic particles over relatively short analytical times, with reasonable accuracy, offers the opportunity to advance partitioning of $b(\lambda)$ (Eq. 1) as well as $b_{\mathrm{m}}(\lambda)$. This has value for many Case 2 marine systems (Babin et al. 2003; Mobley et al. 2004) as well as lakes and reservoirs (Kirk 1985; Effler et al. 2002*b*; Peng and Effler 2005), where inorganic particles are important or even dominant in regulating AOPs. Evaluations and projections of the role of minerogenic particles in contributing to $b(\lambda)$ (Babin et al. 2003) and influencing AOPs would be enhanced through inclusion of SAX results as a form of ground truth for model assumptions. SAX results could be particularly valuable in supporting the development and test of inversion models, with goals of characterizing the particle population through measurements of scattering or related attributes (Twardowski et al. 2001; Sullivan et al. 2005).

Expansion of application of SAX for inland waters could have particular value for individual systems where extensive rehabilitation technologies are under evaluation to achieve improvements in water clarity. Application of SAX can support identification of the appropriate attenuating constituent target(s) and establishment of reasonable expectations for implementation of management actions; for example, erosion control could provide greater benefits than reduction in nutrient loading in some systems (Kirk 1985; Effler et al. 2001*a*, 2002*a*). SAX will also have utility for a broader array of freshwaters by supporting initiatives to expand the capabilities of remote sensing for inland waters (Mikkelsen 2002; Pierson and Strömbeck 2000).

Additional SAX characterizations are needed, in concert with appropriate optical measurements, to establish the representativeness of findings presented here, particularly with respect to PSDs and closure for the independent estimates of $b_{\mathrm{m}}(\lambda)$. Given the lack of minerogenic particle information, broad surveys with SAX that include characterization of all the light-scattering attributes would have substantial value. PSDs deserve particular attention with respect to appropriate functional representations and their applicability. Many inland waters can be expected to demonstrate more complex temporal patterns, associated with multiple sources and drivers, in minerogenic particle composition and PAV_m than those observed in this study. For example, many hard-water alkaline lakes experience seasonal precipitation (autochthonous input) of calcite, which may superimpose onto a signature of external loading (allochthonous inputs) of terrigenous minerals (Weidemann et al. 1985; Peng and Effler 2005). Future closure efforts for $b_m(\lambda)$ estimates from SAX characterizations will probably be most effectively advanced through continued focus on systems where minerogenic particles dominate $b(\lambda)$.

References

Agrawal, Y. C., and H. C. Pottsmith. 2000. Instruments for particle size and settling velocity observations in sediment transport. Mar. Geo. **168:** 89–114.

Babin, M., A. Morel, V. Fournier-Sicre, F. Fell, and D. Stramski. 2003. Light scattering properties of marine particles in coastal and open ocean waters as related to the particle mass concentration. Limnol. Oceanogr. **48:** 843–859.

Bader, H. 1970. The hyperbolic distribution of particle sizes. J. Geophys. Res. **75:** 2822–2830.

Bohren, C. F., and D. R. Huffman. 1983. Absorption and scattering of light by small particles. Wiley.

Boss, E., and others. 2001. Spectral particulate attenuation and particle size distribution in the bottom boundary layer of a continental shelf. J. Geophys. Res. **106** (C5): 9509–9516.

Bricaud, A., A. Morel, and L. Prieur. 1983. Optical efficiency factors of some phytoplankters. Limnol. Oceanogr. **28:** 816–832.

Bukata, R. P., J. H. Jerome, K. Y. Kondratyev, and D. V. Pozdnyakov. 1995. Optical properties and remote sensing of inland and coastal waters. CRC Press.

Carder, K. L., G. F. Beardsley, Jr., and H. Pak. 1971. Particle size distributions in the eastern equatorial Pacific. J. Geophys. Res. **76:** 5070–5077.

Clesceri, L. S., A. E. Greenberg, and A. D. Eaton [eds.] 1998. Standard methods for the examination of water and wastewater, 20th ed. American Public Health Association, American Water Works Association, Water Environment Federation.

Davies-Colley, R. J., and D. G. Smith. 2001. Turbidity, suspended sediment, and water clarity: A review. J. Am. Water Resour. Assoc. **37:** 1085–1102.

Effler, S. W., R. K. Gelda, J. A. Bloomfield, S. O. Quinn, and D. L. Johnson. 2001*a*. Modeling the effects of tripton on water clarity: Lake Champlain. J. Water Resour. Plann. Manage. **127:** 224–234.

———, D. L. Johnson, J. F. Jiao, and M. G. Perkins. 1992. Optical impacts and sources of suspended solids in Onondaga Creek, USA. Water Resour. Bull. **28:** 251–262.

———, C. M. Matthews, and D. A. Matthews. 2001*b*. Patterns of gross deposition in reservoirs enriched in inorganic tripton. Can. J. Fish. Aquat. Sci. **58:** 2177–2188.

———, and D. A. Matthews. 2004. Sediment resuspension and drawdown in a water supply reservoir. J. Am. Water Resour. Assoc. **40:** 251–264.

———, ———, M. G. Perkins, D. L. Johnson, F. Peng, M. R. Penn, and M. T. Auer. 2002*a*. Patterns and impacts of inorganic tripton in Cayuga Lake. Hydrobiologia **482:** 137–150, doi:10.1023/A:1021264415323.

———, A. P. Prestigiacomo, F. Peng, K. B. Bulygina, and D. G. Smith. 2006. Resolution of turbidity patterns from runoff events in a water supply reservoir, and the advantage of *in situ* beam attenuation measurements. Lake Reserv. Manage. **22:** 79–93.

———, and others. 2002*b*. Tripton, transparency and light penetration in seven New York reservoirs. Hydrobiologia **468:** 213–232, doi:10.1023/A:1015285231381.

Egan, W. G., and T. W. Hilgeman. 1979. Optical properties of inhomogeneous materials: Applications to geology, astronomy, chemistry, and engineering. Academic Press.

Gallegos, C. L., D. L. Correll, and J. W. Pierce. 1990. Modeling spectral diffuse attenuation, absorption, and scattering coefficients in a turbid estuary. Limnol. Oceanogr. **35:** 1486–1502.

Gordon, H. R., and T. Du. 2001. Light scattering by nonspherical particles: Application to coccoliths detached from *Emiliania huxleyi*. Limnol. Oceanogr. **46:** 1438–1454.

Holland, A. C., and G. Gagne. 1970. The scattering of polarized light by polydisperse systems of irregular particles. Appl. Opt. **9:** 1113–1121.

Iturriaga, R., and D. A. Siegel. 1989. Microphotometric characterization of phytoplankton and detrital absorption properties in the Sargasso Sea. Limnol. Oceanogr. **34:** 1706–1776.

Johnson, D. L., J. Jiao, S. G. DosSantos, and S. W. Effler. 1991. Individual particle analysis of suspended materials in Onondaga Lake, New York. Environ. Sci. Technol. **25:** 736–744.

Jonasz, M. 1987. Nonsphericity of suspended marine particles and its influence on light scattering. Limnol. Oceanogr. **32:** 1059–1065.

———, and G. Fournier. 1996. Approximation of the size distribution of marine particles by a sum of log-normal functions. Limnol. Oceanogr. **41:** 744–754.

Keen, T. R., and R. H. Stavn. 2000. Developing a capability to forecast coastal ocean optics: Minerogenic scattering, p. 178–193. *In* M. L. Spaulding and H. L. Butler [eds.], 6th Int. Conf. Estuarine and Coastal Modeling. American Society of Civil Engineering.

Kirk, J. T. O. 1985. Effects of suspensoids (turbidity) on penetration of solar radiation in aquatic ecosystems. Hydrobiologia **125:** 195–208, doi:10.1007/BF00045935.

———. 1994. Light and photosynthesis in aquatic ecosystems. Cambridge University Press.

Lal, D., and A. Lerman. 1975. Size spectra of biogenic particles in ocean water and sediments. J. Geophys. Res. **80:** 423–430.

Lambert, C. E., C. Jehanno, N. Silverberg, J. C. Brun-Cottan, and R. Chesselet. 1981. Log-normal distributions of suspended particles in the open ocean. J. Mar. Res. **39:** 77–98.

Mikkelsen, O. A. 2002. Variation in the projected surface area of suspended particles: Implications for remote sensing assessment of TSM. Remote Sens. Environ. **79:** 23–29.

Mishchenko, M. I., and L. D. Travis. 1994. Light scattering by polydispersions of randomly oriented spheroids with sizes comparable to wavelengths of observation. Appl. Opt. **33:** 7206–7225.

Mobley, C. D. 1994. Light and water: Radiative transfer in natural waters. Academic Press.

———, D. Stramski, W. P. Bissett, and E. Boss. 2004. Optical modeling of ocean waters: Is the Case 1–Case 2 still useful? Oceanography **17:** 60–67.

Morel, A., and L. Prieur. 1977. Analysis of variations in ocean color. Limnol. Oceanogr. **22:** 709–722.

Mugnai, A., and W. J. Wiscombe. 1989. Scattering from nonspherical Chebyshev particles. 3: Variability in angular scattering patterns. Appl. Opt. **28:** 3061–3073.

Owen, R. W., Jr. 1974. Optically effective area of particle ensembles in the sea. Limnol. Oceanogr. **19:** 584–590.

PAK, H., J. R. V. ZANEVELD, AND G. F. BEARDSLEY, JR. 1971. Mie scattering by suspended clay particles. J. Geophys. Res. **76:** 5065–5069.

PENG, F., AND S. W. EFFLER. 2005. Inorganic tripton in the Finger Lakes of New York: importance to optical characteristics Hydrobiologia **543:** 259–277, doi:10.1007/s10750-004-7892-2.

———, D. L. JOHNSON, AND S. W. EFFLER. 2002. Suspensoids in New York City's drinking water reservoirs: Turbidity apportionment. J. Am. Water Resour. Assoc. **38:** 1453–1465.

———, ———, AND ———. 2004. Characterization of inorganic particles in selected reservoirs and tributaries of the New York City water supply. J. Am. Water Resour. Assoc. **40:** 663–676.

PIERSON, D. C., AND N. STRÖMBECK. 2000. A modelling approach to evaluate preliminary remote sensing algorithms: Use of water quality data from Swedish Great Lakes. Geophysica **36:** 177–202.

PROCTOR, T. D., AND G. W. HARRIS. 1974. The turbidity of suspensions of irregular quartz particles. Aerosol Sci. **5:** 81–90.

RISOVIĆ, D. 1993. Two-component model of sea particle size distribution. Deep-Sea Res. **40:** 1459–1473.

———. 2002. Effect of suspended particulate-size distribution on the backscattering ratio in the remote sensing of seawater. Appl. Opt. **41:** 7092–7101.

———, AND M. MARTINIS. 1995. A comparative analysis of sea-particle-size distribution models. Fizika B **4:** 111–120.

RUSS, J. C. 1998. The image processing handbook, 3rd ed. CRC Press.

STAVN, R. H., AND T. R. KEEN. 2004. Suspended minerogenic particle distributions in high-energy coastal environments: Optical implications. J. Geophys. Res. **109:** C05005, doi: 10.1029/2003JC002098.

STRAMSKI, D., AND S. B. WOŹNIAK. 2005. On the role of colloidal particles in light scattering in the ocean. Limnol. Oceanogr. **50:** 1581–1591.

SULLIVAN, J. M., M. S. TWARDOWSKI, P. L. DONAGHAY, AND S. A. FREEMAN. 2005. Use of optical scattering to discriminate particle types in coastal waters. Appl. Opt. **44:** 1667–1680.

TREWEEK, G. P., AND J. J. MORGAN. 1980. Prediction of suspension turbidities from aggregate size distribution, p. 329–352. *In* M. C. Kevanaugh and J. O. Leckie [eds.], Particulates in water: Characterization, fate, effects and removal. Advances in Chemistry Series. American Chemical Society, Division of Environmental Chemistry.

TWARDOWSKI, M. S., E. BOSS, J. B. MACDONALD, W. S. PEGAU, A. H. BARNARD, AND J. R. V. ZANEVELD. 2001. A model for estimating bulk refractive index from the optical backscattering ratio and the implications for understanding particle composition in case I and case II waters. J. Geophys. Res. **106** (C7): 14129–14142.

VANT, W. N., AND R. J. DAVIES-COLLEY. 1984. Factors affecting clarity of New Zealand lakes. N. Z. J. Mar. Freshw. Res. **18:** 367–377.

VOLTEN, H., AND OTHERS. 1998. Laboratory measurements of angular distributions of light scattered by phytoplankton and silt. Limnol. Oceanogr. **43:** 1180–1197.

WEIDEMANN, A. D., AND T. T. BANNISTER. 1986. Absorption and scattering coefficients in Irondequoit Bay. Limnol. Oceanogr. **31:** 567–583.

———, ———, S. W. EFFLER, AND D. L. JOHNSON. 1985. Particulate and optical properties during $CaCO_3$ precipitation in Otisco Lake. Limnol. Oceanogr. **30:** 1078–1083.

WOŹNIAK, S. B., AND D. STRAMSKI. 2004. Modeling the optical properties of mineral particles suspended in seawater and their influence on ocean reflectance and chlorophyll estimation from remote sensing algorithms. Appl. Opt. **43:** 3489–3503.

YIN, C., AND D. L. JOHNSON. 1984. An individual particle analysis and budget study of Onondaga Lake sediments. Limnol. Oceanogr. **29:** 1193–1201.

Received: 15 February 2006
Accepted: 15 August 2006
Amended: 21 September 2006